



Silicon Isotopic Composition of Mainstream Presolar SiC Grains Revisited: The Impact of Nuclear Reaction Rate Uncertainties

Hung Kwan Fok^{1,6,7} , Marco Pignatari^{2,3,4,7} , Benoît Côte^{2,7} , and Reto Trappitsch^{5,1,7} ¹ Department of Physics, Brandeis University, Abelson-Bass-Yalem 107, Waltham, MA 02453, USA; reto.trappitsch@epfl.ch² Konkoly Observatory, Research Centre for Astronomy and Earth Sciences, HUN-REN, Konkoly Thege M. út 15-17, Budapest 1121, Hungary³ CSFK, MTA Centre of Excellence, Konkoly Thege Miklós út 15-17, Budapest 1121, Hungary⁴ E. A. milne Centre for Astrophysics, University of Hull, Cottingham Road, Kingston upon Hull, HU6 7RX, UK⁵ Laboratory for Biological Geochemistry, School of Architecture, Civil & Environmental Engineering, École Polytechnique Fédérale de Lausanne, GR C2 505, Station 2, 1015 Lausanne, Switzerland

Received 2024 August 23; revised 2024 November 01; accepted 2024 November 12; published 2024 December 5

Abstract

Presolar grains are stardust particles that condensed in the ejecta or in the outflows of dying stars and can today be extracted from meteorites. They recorded the nucleosynthetic fingerprint of their parent stars and thus serve as valuable probes of these astrophysical sites. The most common types of presolar silicon carbide grains (called mainstream SiC grains) condensed in the outflows of asymptotic giant branch stars. Their measured silicon isotopic abundances are not significantly influenced by nucleosynthesis within the parent star but rather represent the pristine stellar composition. Silicon isotopes can thus be used as a proxy for galactic chemical evolution (GCE). However, the measured correlation of $^{29}\text{Si}/^{28}\text{Si}$ versus $^{30}\text{Si}/^{28}\text{Si}$ does not agree with any current chemical evolution model. Here, we use a Monte Carlo model to vary nuclear reaction rates within their theoretical or experimental uncertainties and process them through stellar nucleosynthesis and GCE models to study the variation of silicon isotope abundances based on these nuclear reaction rate uncertainties. We find that these uncertainties can indeed be responsible for the discrepancy between measurements and models and that the slope of the silicon isotope correlation line measured in mainstream SiC grains agrees with chemical evolution models within the nuclear reaction rate uncertainties. Our result highlights the importance of future precision reaction rate measurements for resolving the apparent data–model discrepancy.

Unified Astronomy Thesaurus concepts: Circumstellar grains (239); Stellar nucleosynthesis (1616); Reaction rates (2081); Galaxy chemical evolution (580); Isotopic abundances (867)

1. Introduction

Presolar grains are small particles that condensed in the outflows of dying stars. After they drifted through the interstellar medium (ISM), some of them were incorporated into the first condensing solids in the solar nebula and thus into meteorite precursors. Today, these grains can be extracted from primitive meteorites, i.e., meteorites that were never altered during the 4.567 Gyr since the solar system formed (e.g., L. R. Nittler & F. Ciesla 2016). Presolar grains recorded the nucleosynthesis fingerprint of their parent stars at the time and in the region where the particles condensed. Analyzing them thus allows us to directly probe the isotopic composition of these astrophysical sites.

Currently, the best-studied presolar phase is SiC grains, mainly since they occur in sizes of up to several micrometers and are thus relatively large compared to, e.g., presolar silicates, and since their chemical makeup is strong enough such that they can be separated from the meteoritic host material by etching with strong acids (S. Amari et al. 1994). This latter point is also highly effective in removing any solar system contamination from these particles, such that the pristine stellar material can be measured without significant dilution with solar system material (N. Liu et al. 2014). The majority of presolar SiC grains, known as mainstream grains,

condensed in the outflows of low-mass stars (up to a few solar masses) when they underwent the asymptotic giant branch (AGB) phase at the end of their lives. These stars have been observed to produce slow neutron-capture process (*s*-process) nuclei (e.g., P. W. Merrill 1952), and the same observations have also been confirmed in SiC mainstream grains (M. R. Savina et al. 2004), showing the provenance of these grains. The *s*-process mainly produces isotopes heavier than iron (e.g., R. Gallino et al. 1998). Below iron, presolar SiC mainstream grains show isotopic compositions of certain elements, e.g., silicon and titanium, that represent the original composition the parent star started out with. Indeed, the intrinsic nucleosynthesis processes in the grain’s parent AGB stars are not expected to introduce significant anomalies in the isotopic composition of these species (D. D. Clayton & F. X. Timmes 1997; C. M. O’D. Alexander & L. R. Nittler 1999).

The silicon isotopic ratios of the majority of the SiC mainstream grains are enriched in the secondary isotopes ^{29}Si and ^{30}Si compared to the solar system. Within a classic galactic chemical evolution (GCE) scenario (e.g., C. Kobayashi et al. 2020), the silicon isotopes of these grains would indicate that their parent stars were more evolved in terms of GCE compared to the solar system. Furthermore, the correlation of $\delta^{29}\text{Si}_{28}$ versus $\delta^{30}\text{Si}_{28}$ ⁸ as measured

⁶ Present address: Morton K. Blaustein Department of Earth & Planetary Sciences, Johns Hopkins University, Olin Hall, 3300 San Martin Drive, Baltimore, MD 21218, USA.

⁷ NuGrid collaboration, <https://nugridstars.org>.

⁸ Throughout this Letter, we express silicon isotope ratios as δ -values. These are defined as

$$\delta^i\text{Si}_{28} = \delta\left(\frac{^i\text{Si}}{^{28}\text{Si}}\right) = \left[\frac{(^i\text{Si}/^{28}\text{Si})_m}{(^i\text{Si}/^{28}\text{Si})_{\odot}} - 1\right] \cdot 1000 \quad (\text{‰}). \quad (1)$$

Here, i is the mass number of the minor silicon isotopes ($i \in \{29, 30\}$). Subscripts “m” and “ \odot ” refer to the model output/presolar grain measurements and solar abundances of the given isotopes, respectively. Overall, δ -values represent the deviation of a modeled or measured value from the solar isotope ratio (K. Lodders 2021) in permil.



Original content from this work may be used under the terms of the [Creative Commons Attribution 4.0 licence](https://creativecommons.org/licenses/by/4.0/). Any further distribution of this work must maintain attribution to the author(s) and the title of the work, journal citation and DOI.

in presolar grains is significantly larger than predictions of GCE models. While the linear correlation along the mainstream line predicts a slope of 1.342 ± 0.004 (T. Stephan et al. 2024), typical homogeneous GCE models predict correlation lines with a slope of around unity (e.g., D. D. Clayton & F. X. Timmes 1997). For clarity, we will subsequently refer to the SiC mainstream grain correlation line as the “mainstream line” and the analogous GCE model-predicted correlation line as the “GCE line.” Numerous studies have sought to resolve this model–data discrepancy. D. D. Clayton & F. X. Timmes (1997) proposed an explanation for the slope of the mainstream line, suggesting that the Sun is significantly enriched in ^{30}Si compared to the typical ISM. However, this explanation requires the parent stars of the mainstream grains to experience a more extensive dredge-up of He-shell materials, which contradicts the $^{12}\text{C}/^{13}\text{C}$ ratios in the mainstream grains (C. M. O’D. Alexander & L. R. Nittler 1999). M. Lugaro et al. (1999) illustrated that a heterogeneous GCE predicts a slope higher than the typical homogeneous GCE model but still lower than the slope of the mainstream line. An alternative theory was introduced by D. D. Clayton (2003), who postulated that the silicon isotopic ratio in the mainstream grains might represent the mixing line of a merger between a dwarf galaxy and the Milky Way disk before the formation of the solar system. However, this model remains speculative and lacks concrete evidence.

In this study, we approach the problem from a nuclear physics perspective. Previous studies suggested that uncertainties in nuclear reaction rates might explain the discrepancy between the GCE model predictions and mainstream grain measurements (F. X. Timmes & D. D. Clayton 1996). F. X. Timmes & D. D. Clayton (1996) came to this conclusion by analyzing GCE models in comparison with presolar SiC mainstream grains. They could not find an agreement between model and data but speculated that nuclear reaction rate uncertainties could play a major role.

While silicon is mainly produced in core-collapse supernovae (CCSNe; e.g., C. Kobayashi et al. 2020), presolar grains from AGB stars, e.g., mainstream SiC grains, trace the GCE-averaged signal of all CCSNe. E. Zinner et al. (2006) studied the silicon isotopic composition of SiC Z grains, which were hypothesized to have formed in low-mass, low-metallicity AGB stars (P. Hoppe et al. 1997). These grains are characterized by elevated $^{30}\text{Si}/^{28}\text{Si}$ ratios compared to SiC mainstream grains. E. Zinner et al. (2006) concluded for the used AGB star nucleosynthesis models that using the neutron-capture reaction rates by K. H. Guber et al. (2003) yields a better agreement with the SiC Z-grain measurements than when using the rates by Z. Y. Bao et al. (2000).

P. Hoppe et al. (2009) analyzed presolar SiC X grains, which condensed in the ejecta of CCSNe. Each of these samples thus only probes one individual CCSN event, and the grain’s silicon isotopic composition does not represent the average GCE signal. By analyzing SiC X grains, P. Hoppe et al. (2009) found that they can explain all isotopic measurements except for the abundance of ^{29}Si rather well with existing CCSN models. However, in order to match the ^{29}Si measurements, they needed to boost its production in the model. Enhancing the $^{26}\text{Mg}(\alpha, n)^{29}\text{Si}$ reaction rate in the explosive carbon- and oxygen-burning calculations by a factor of 3 led to a good match of measurements and models.

The studies by E. Zinner et al. (2006) and P. Hoppe et al. (2009) highlight the high potential impact of nuclear uncertainties on nucleosynthesis models, and consequently, we expect a similar effect on GCE models of silicon isotopes. Notably, the increased $^{29}\text{Si}/^{30}\text{Si}$ ratio shown in P. Hoppe et al. (2009) might elevate the GCE line and potentially resolve the model–data discrepancy. In this Letter, we quantify, for the first time, the impact of nuclear uncertainties on the GCE of silicon isotopes using a Monte Carlo (MC) framework.

2. Methods and Model

In this section, we first discuss the uncertainties of the relevant nuclear reaction rates leading to the production and destruction of silicon isotopes. Then, we present models used to estimate the impact of nuclear reaction rate uncertainties on the GCE of silicon isotopes.

2.1. Nuclear Reaction Rates and Their Uncertainties

Nuclear reaction rates are a key input for nucleosynthesis in stellar evolution models. Their uncertainties are propagating through the stellar simulations and into the results of GCE (Figure 1). In this work, we focus solely on the effects of nuclear uncertainties on the GCE of silicon isotopes.

We concentrate our uncertainty study on the specific region in CCSNe where silicon isotopes are produced. Mass coordinates for the individual zones are given in Appendix A. The main paths to produce and destroy silicon in this region are via the reactions shown in Table 1. To determine these main reactions, we consider the contribution of each individual reaction rate to the sum total of reactions in the analyzed stellar zones. The reactions named in Table 1 are the ones that change the silicon isotopic composition by δ_i such that $|\delta_i/\delta_{\max}| \geq 0.001$, where $\delta_{\max} = \max(\{\delta_i; i = \text{a reaction in the network}\})$. For each nuclear reaction rate, the table presents the upper and lower limit of the associated uncertainties. For measured reaction rates, we use $\pm 2\sigma$ for the uncertainty in our model, where σ represents the analytical one standard deviation uncertainty. For reaction rates that were not measured and for which thus only theoretical values and no uncertainties exist, we employ the same uncertainties that were used by T. Rauscher et al. (2016).

For the $^{28,29,30}\text{Si}(n, \gamma)$ nuclear reaction rates, we performed nucleosynthesis calculations using two distinct sets of rates, namely, the ones from Z. Y. Bao et al. (2000) and K. H. Guber et al. (2003). While the K. H. Guber et al. (2003) rates were used in the nucleosynthesis calculations by, e.g., E. Zinner et al. (2006) and C. Ritter et al. (2018b), these rates are still controversial, in particular for ^{30}Si . We therefore use the rates by K. H. Guber et al. (2003) as the standard case to discuss the effect of nuclear reaction rate uncertainties on the GCE of silicon isotopes and compare our final results with a second set of simulations using the rates by Z. Y. Bao et al. (2000). Uncertainties for both sets are given in Table 1.

2.2. Models

We developed a nucleosynthesis–GCE MC framework to quantify the effect of nuclear uncertainties on the stellar yields of their respective stars and consequently on the results of GCE. Figure 1 shows an overview of the parts that are important for this work. The framework can be separated into two submodels: the stellar model and the galaxy model.

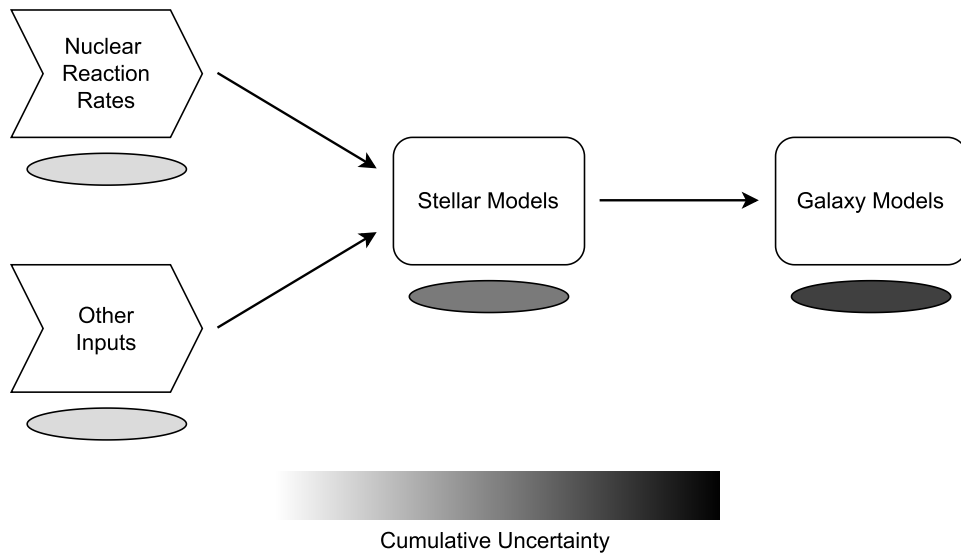


Figure 1. Schematic overview of the GCE pipeline that we employ in this work to study the effects of nuclear reaction rate uncertainties on the evolution of silicon isotopes in the Milky Way. The gray scale shows schematically how uncertainties propagate through the model and how small initial uncertainties can have a large effect on predicting isotopic compositions.

Table 1

Uncertainty Factors Used in This Work for Considered Nuclear Reaction Rates

Reaction	U^{hi}	U^{lo}	Type ^a
$^{28}\text{Si} (n, \gamma)^{29}\text{Si}$	1.18 ^b /1.21 ^c	0.82 ^b /0.79 ^c	exp
$^{29}\text{Si} (n, \gamma)^{30}\text{Si}$	1.20 ^b /1.23 ^c	0.80 ^b /0.77 ^c	exp
$^{30}\text{Si} (n, \gamma)^{31}\text{Si}$	1.36 ^b /1.18 ^c	0.64 ^b /0.82 ^c	exp
$^{24}\text{Mg} (\alpha, \gamma)^{28}\text{Si}$	1.3	0.7	exp
$^{25}\text{Mg} (\alpha, n)^{28}\text{Si}$	2.000	0.100	th
$^{26}\text{Mg} (\alpha, n)^{29}\text{Si}$	2.000	0.100	th
$^{32}\text{S} (n, \alpha)^{28}\text{Si}$	2.000	0.100	th
$^{33}\text{S} (n, \alpha)^{29}\text{Si}$	2.000	0.100	th

Notes. For the upper and lower limits of the considered uncertainties, the reaction rates are multiplied by U^{hi} and U^{lo} , respectively. For experimentally determined reaction rates, 2σ uncertainties were used as the upper and lower limits. For theoretical rates, we use the same uncertainties as T. Rauscher et al. (2016).

^a exp: experimentally determined rates; th: theoretically determined rates.

^b Uncertainties as reported by K. H. Guber et al. (2003).

^c Uncertainties as reported by Z. Y. Bao et al. (2000).

The stellar evolution calculation is the starting point of our framework. Here, we utilize the NuGrid stellar models by C. Ritter et al. (2018b), whose 1D stellar evolution calculations were done with the MESA stellar evolution code (rev. 3372; B. Paxton et al. 2011, 2013, 2015). CCSN explosions are based on the semianalytical approach presented in M. Pignatari et al. (2016). The thermodynamic and structural information of the stellar evolution calculation and the CCSN explosion model are then extracted and postprocessed using the multizone nuclear reaction network `mppnp` for the nucleosynthesis calculation using a full nuclear reaction rate network (C. Ritter et al. 2018b).

The resulting stellar yields are the input for the galaxy model. Here, we use the two-zone semianalytical galaxy model OMEGA+ (B. Côté et al. 2017, 2018). OMEGA+ consists of a star-forming region, representing the galaxy, surrounded by a hot gas reservoir filling the dark matter halo of the host galaxy and takes a set of galaxy parameters and stellar yields to

calculate the evolution of elemental and isotopic abundances in the galaxy as a function of time. The input parameters of the OMEGA+ calculations were calibrated to reproduce the current bulk properties of the Milky Way (B. Côté et al. 2019). The parameter values are equivalent to the values in the “best” model of B. Côté et al. (2019) and are identical to the values used in by K. A. Womack et al. (2022). Different sets of CCSN yields are adopted to generate the GCE models presented in this work, namely, C. Ritter et al. (2018b), K. Nomoto et al. (2013), and M. Limongi & A. Chieffi (2018). The largest stellar masses available are $M = 25 M_{\odot}$, $40 M_{\odot}$ and $120 M_{\odot}$, respectively. For consistency, the maximum contributing stellar mass adopted for all GCE simulations is $M = 120 M_{\odot}$, which is the largest stellar model provided by M. Limongi & A. Chieffi (2018). For the other GCE models using yields by K. Nomoto et al. (2013) and C. Ritter et al. (2018b), we use the standard extrapolation setup in OMEGA+, i.e., applying the yields of the most massive model available to all more massive stars.

The theoretical and experimental nuclear reaction rates were randomly varied within their uncertainties using a uniform distribution. This approach is identical to the one chosen by T. Rauscher et al. (2016). While experimental reaction rate uncertainties are generally better described using a Gaussian distribution, our results show that systematic differences between different studies play a larger effect than reaction rate uncertainties. Nucleosynthesis within the silicon production CCSN zone for each star is then calculated. This allows us to propagate the uncertainties of the nuclear reaction rates to the total stellar yields. We then input the modified stellar yield into the galaxy model to determine the uncertainties of the GCE model. This means that for each MC iteration, a set of rate variation factors μ_{rate} for the rates of all the reactions shown in Table 1 are randomly generated according to a uniform distribution within the uncertainty limits defined in Table 1. In order to perform a statistically sufficient number of MC calculations, postprocessing the full stellar nucleosynthesis for each set of modified reaction rates is computationally prohibitive. Therefore, for all stellar models, we take representative 1D temperature, plasma-density trajectories from

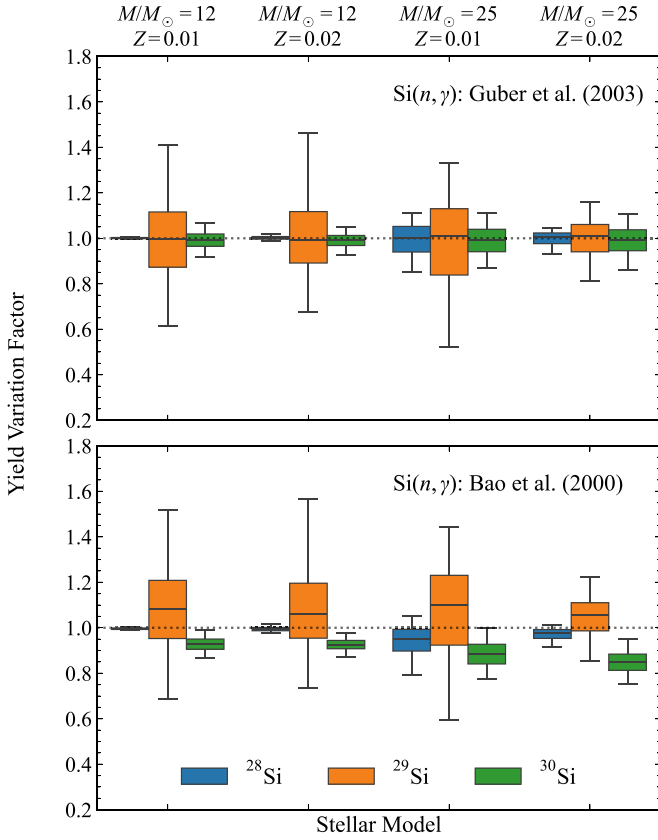


Figure 2. Silicon isotope integrated stellar yield variations for the $12 M_{\odot}$ and $25 M_{\odot}$ stars at $Z = 0.01$ and $Z = 0.02$. The dotted horizontal line indicates the unmodified stellar yields. The variations in the integrated yields are shown as boxes and bars for the 50% and 95% confidence interval, respectively. The top panel shows the yield variation factors using the $\text{Si}(n, \gamma)$ rates by K. H. Guber et al. (2003), and the bottom panel uses the rates by Z. Y. Bao et al. (2000). Note that the dashed line at unity represents in both cases the original stellar models, which used the $\text{Si}(n, \gamma)$ rates by K. H. Guber et al. (2003). Clearly, the largest effects due to nuclear reaction rate uncertainties are seen in ^{29}Si .

their respective explosive silicon production zones, ranging from mass coordinates m_a to m_b (details are given in Appendix B). The subscript represents the index of the computational grid of the MESA stellar evolution code, where 0 represents the center of the star. Each trajectory traces temperature T and plasma density ρ at mass coordinate m_n over time from the onset of core collapse ($t = 0$) to explosion completion ($t = t_f$). The isotope yield scale factor, i.e., the enhancement factor with respect to the trajectory with unmodified reaction rates, λ_n , at each trajectory’s mass coordinate m_n is then computed. For any m_i , the scale factor λ_i is furthermore determined by linear interpolation between the closest neighbors. For $i < a$ or $i > b$, $\lambda_i = 1$. The integrated stellar nucleosynthesis yield for an isotope is then computed by summation as follows:

$$m = \sum_{i=k}^{M-1} \lambda_i X_i \Delta m_i. \quad (2)$$

Here, m_k is the mass cut derived from C. L. Fryer et al. (2012), X_i is the isotopic mass fraction in the stellar nucleosynthesis models in C. Ritter et al. (2018b), and $\Delta m_i = m_{i+1} - m_i$. The yield variation factor ν_{yield} is then calculated as the mass of the total modified yield divided by the mass of the unmodified yield (C. Ritter et al. 2018b). These rate variation factors are

mapped to a set of yield variation factors, ν_{yield} , for all massive star models and all silicon isotopes ^{28}Si , ^{29}Si , and ^{30}Si . Finally, the set of yield variation factors ν_{yield} is passed into OMEGA+ to calculate the GCE of silicon isotopes corresponding to the set of rate variation factors μ_{rate} . This whole process was then repeated for the next set of randomly varied nuclear reaction rates.

Overall, we propagated nuclear reaction rate uncertainties via the described MC approach through eight stellar models. Specifically, we modeled four masses ($12, 15, 20,$ and $25 M_{\odot}$) at two different metallicities ($Z = 0.01$ and 0.02). The models by C. Ritter et al. (2018b) are based on initial abundances scaled to the solar abundances by N. Grevesse & A. Noels (1993; $Z = 0.019$), and the $Z = 0.02$ cases are the closest models to this solar metallicity. More modern solar references are included between $Z = 0.01$ and $Z = 0.02$ (e.g., K. Lodders 2021; E. Magg et al. 2022). The models at these metallicities are the best to use to explore the impact of nuclear uncertainties on the production in CCSNe of Si isotopes. For ^{28}Si , its production is primary; therefore, the initial metallicity of the models does not significantly affect the results. But ^{29}Si and ^{30}Si are mostly secondary-like products, and their production tends to increase with the initial metallicity of the star (e.g., M. Limongi & A. Chieffi 2018; C. Ritter et al. 2018b). Therefore, for the GCE to produce the Si solar abundances and the population of presolar grains, the mildly subsolar and solar-like metallicity models will be representative of all the Si isotopes. For the GCE calculations, the full suite of stellar models from C. Ritter et al. (2018b) is considered. Additional masses required for the GCE calculation are inter-/extrapolated from nearby models as a function of metallicity (see B. Côté et al. 2017).

3. Result and Discussion

3.1. Stellar Nucleosynthesis Uncertainties

To determine the impact of nuclear reaction rate uncertainties on the GCE of silicon isotopes, we performed 10,000 MC simulations to vary the nuclear reaction rates that lead to the production and destruction of silicon isotopes following the procedure described in Section 2. Convergence of our MC model is discussed in Appendix C. The key inputs for the GCE model are the overall stellar yields; thus, the uncertainty of these models is determined by the integrated variations in silicon isotopic yields. Figure 2 shows the variations of the silicon isotopic massive star yields due to nuclear reaction rate uncertainties for selected massive star models using $\text{Si}(n, \gamma)$ rates by K. H. Guber et al. (2003; top) and Z. Y. Bao et al. (2000; bottom). Details on variations with the stellar zones are provided in Appendix D. Boxes in Figure 2 depict the 50% confidence intervals of the variation in integrated stellar yields, while bars show the 95% confidence interval. Clearly, the ^{29}Si yields show the largest variations. While for the $12 M_{\odot}$ star, the variation factors of ^{29}Si are more than a factor of 1.3 higher than for all other isotopes, the difference is significantly lower for the $25 M_{\odot}$ star. This effect is due to the fallback radius in the $25 M_{\odot}$ stars being larger than in the $12 M_{\odot}$ stars. The $25 M_{\odot}$ stars therefore eject significantly less silicon from the center and thus recycle less material back into the galaxy. Therefore, silicon modified in the explosion contributes a larger part of the overall yield, which results in the larger variation factors for all silicon isotopes. Note that the variation factors shown in

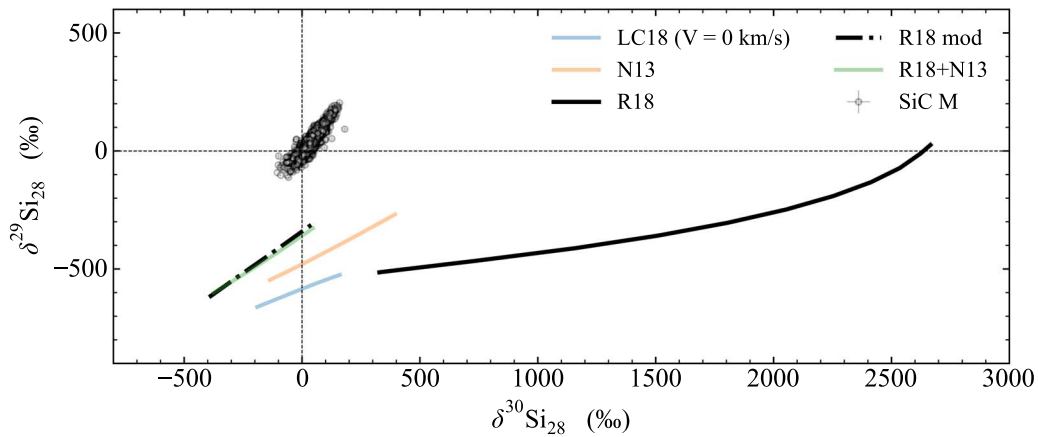


Figure 3. Comparison of GCE model predictions of silicon isotope evolution using different stellar yield sets with presolar SiC mainstream grains (SiC M). The simulated time range is between 4.2 Ga prior to solar system formation (left-hand side of the model lines) up to solar system formation (right-hand side of model lines). Citation key: N13—K. Nomoto et al. (2013), LC18—M. Limongi & A. Chieffi (2018), R18—C. Ritter et al. (2018b). Presolar grain measurements are taken from the presolar grain database (T. Stephan et al. 2024).

Figure 2 are not weighted by the overall yields. Thus, the overall contribution of the individual stars to GCE cannot be derived from this figure.

3.2. GCE Models and Propagated Uncertainties

The stellar structure and nucleosynthesis yields in the models by C. Ritter et al. (2018b) are heavily affected by the convective O–C shell merger during silicon shell burning, which occurs in some of the stellar models. For example, C. Ritter et al. (2018a) demonstrate that burning of ingested neon during the shell mergers results in a boost of odd- Z elements and, when propagated through a GCE model, results in large overproduction factors for these elements of up to a factor of 10. We find that O–C shell mergers greatly affect the production of Si isotopes in massive stars and also have a clear impact on our GCE results.

For example, the ^{30}Si yield in the $15 M_{\odot}$, $Z = 0.02$ model of C. Ritter et al. (2018b) is about 10 times higher than the ^{30}Si yield predicted by other massive star models that do not undergo a convective O–C shell merger (K. Nomoto et al. 2013; M. Limongi & A. Chieffi 2018). In Figure 3, we compare the OMEGA+ predictions using the stellar yield set of C. Ritter et al. (2018b) with the predictions using the stellar yield sets of other massive star models by K. Nomoto et al. (2013) and M. Limongi & A. Chieffi (2018).

The stellar models of C. Ritter et al. (2018b) significantly overproduce ^{30}Si compared to other stellar models in GCE. However, at the same time, they are the sole models that reproduce the measured $^{29}\text{Si}/^{28}\text{Si}$ isotope ratios. This is a direct result of the O–C shell mergers that occur in the $15 M_{\odot}$ and $20 M_{\odot}$ stars in these models. On the other hand, GCE predictions using stellar yields by K. Nomoto et al. (2013) and M. Limongi & A. Chieffi (2018) generally agree well with each other, underproducing ^{29}Si compared to both the Sun and the presolar grains sample. This is a well-known issue found by previous GCE studies focused on the Si isotopes (e.g., M. Lugaro et al. 1999).

The occurrence of O–C shell mergers and the accuracy of the 1D model predictions are highly uncertain. Other massive star models do not show the occurrence of O–C shell mergers, or they show them at different progenitor masses and/or metallicities. The overall nucleosynthesis impact may also vary strongly

between different models (e.g., see L. Roberti et al. 2024). Moreover, C. Ritter et al. (2018b) show that a major O–C shell merger in the $M/M_{\odot} = 15$, $Z = 0.02$ model disappears in higher-resolution simulations. In general, large-scale asymmetries arising in the 3D calculations of the O–C shell merger in R. Andrassy et al. (2020) suggest that 1D spherically symmetric models cannot capture the behavior of the shell merger.

We performed two test cases to demonstrate the effect of the O–C shell merger on silicon isotopes. In the first test case, we substituted the stellar yields of the $M/M_{\odot} = 15$, 20 , $Z = 0.01$, 0.02 models, with values given by linear interpolations of the yields of the nearby models (i.e., $M/M_{\odot} = 12$, 25 , $Z = 0.01$, 0.02). This interpolation is based on the default OMEGA+ assumption that yields depend linearly on the initial mass and metallicity of the stellar model. This test case is shown as a dashed–dotted line in Figure 3 labeled “R18 mod.” In the second test case, we substituted the stellar yields of the $M/M_{\odot} = 15$, 20 , $Z = 0.01$, 0.02 models with yields from K. Nomoto et al. (2013), shown as the green line labeled “R18 +N13” in Figure 3. We find that the two test cases yield almost identical results with respect to the GCE of silicon isotopes. Moreover, the resulting GCE curves of the two test cases show $\delta^{30}\text{Si}_{28}$ values that are similar to the $\delta^{30}\text{Si}_{28}$ values of the GCE curves using stellar yield sets by K. Nomoto et al. (2013) and M. Limongi & A. Chieffi (2018).

Coming back to the comparison with the solar abundances and the Si isotopic ratios in presolar SiC mainstream measurements, two main issues arise from GCE simulations: (1) the models do not reproduce the heavy silicon isotopic compositions measured in presolar SiC mainstream grains, and (2) the slope of all GCE models is significantly shallower than the measured slope. F. X. Timmes & D. D. Clayton (1996) already discussed these issues and stated that accumulated uncertainties will always result in models having difficulties in reproducing the precise isotopic composition of presolar grain measurements. A further issue represents itself in the fact that these grains seem enriched in secondary $^{29,30}\text{Si}$ when compared with solar. Therefore, a simple GCE model based on the age–metallicity relation will never be able to explain the measured enhancement in $^{29,30}\text{Si}$ with respect to solar, since the model will, by definition, end up at solar composition at the time of birth of the solar nebula. Only heterogeneous GCE models (e.g., M. Lugaro et al. 1999; L. R. Nittler 2005) have the

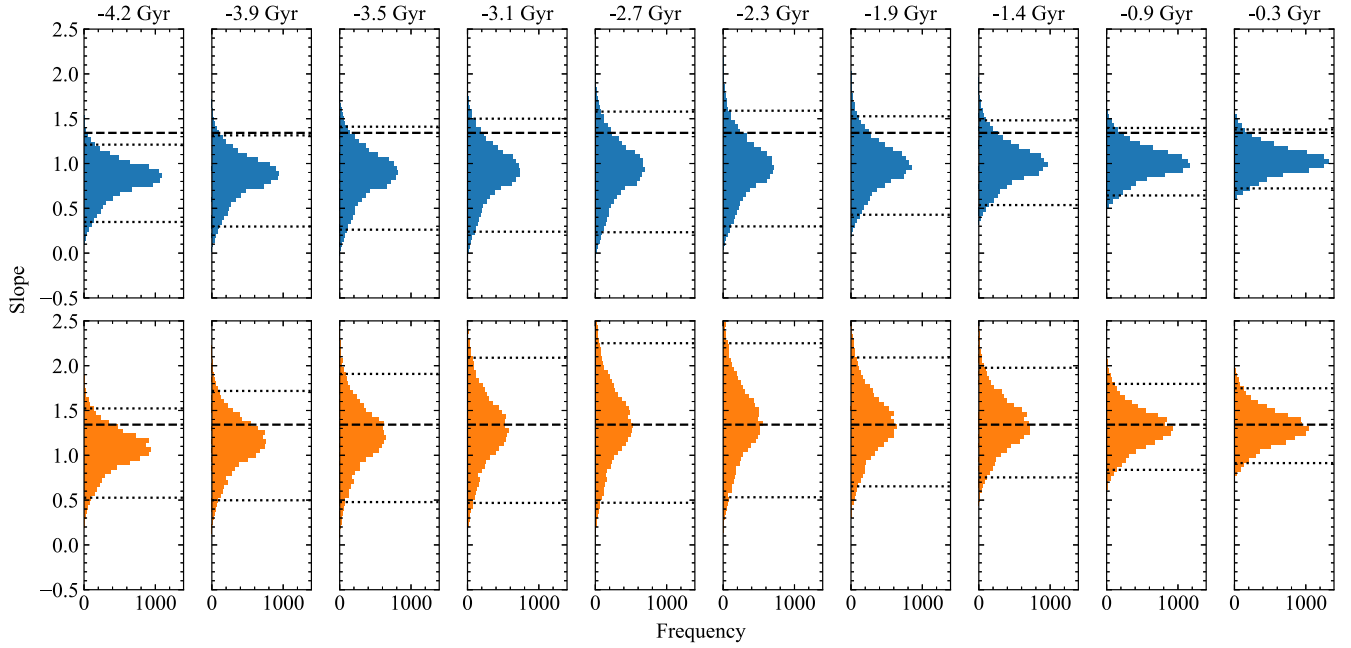


Figure 4. Slope distribution of the silicon isotope correlation line based on varying the nuclear reaction rates within the described uncertainties. Each histogram was calculated at a given time in GCE history prior to solar system formation. Dotted lines represent the 95% confidence intervals, while the dashed line shows the measured slope by analyzing presolar SiC mainstream grains (T. Stephan et al. 2024). The top histograms (blue) show the slope distribution when using the $^{28,29,30}\text{Si}$ (n, γ) rates by K. H. Guber et al. (2003), and the bottom histograms (orange) use the rates by Z. Y. Bao et al. (2000).

potential of predicting the measured isotope ratios. F. X. Timmes & D. D. Clayton (1996), however, also pointed out that the slope of the predicted GCE silicon isotope correlation line is approximately 1, i.e., significantly lower than the measured mainstream line. They suggested that this discrepancy could likely be due to nuclear reaction rate uncertainties. In fact, we see that the modified C. Ritter et al. (2018b) models predict a slope of approximately 1. Other stellar yields by K. Nomoto et al. (2013) and M. Limongi & A. Chieffi (2018) result in an even shallower slope, increasing the discrepancy.

Using the modified C. Ritter et al. (2018b) stellar yields (“R18 mod” in Figure 3), we calculated the uncertainties of the slope of the silicon GCE correlation line due to nuclear reaction rate uncertainties. We varied the stellar yields of the $M/M_{\odot} = 12, 25, Z = 0.01, 0.02$ models based on the MC results shown in Section 3.1. While the individual rates were varied independently from each other, the same rate variations for any given run are consistently used across the different stellar masses and metallicities that we modeled. The stellar yields of the $M/M_{\odot} = 15, 20, Z = 0.01, 0.02$ models were then interpolated based on the modified yields of the $M/M_{\odot} = 12, 25, Z = 0.01, 0.02$ models. Figure 4 compares the variations of the slope of the silicon GCE line with the slope of the line predicted by mainstream SiC grains. The top row shows the slope predictions using the $^{28,29,30}\text{Si}$ (n, γ) rates by K. H. Guber et al. (2003), and the bottom row uses the rates by Z. Y. Bao et al. (2000). Both sets of reaction rates were varied within their respective experimental uncertainties (Table 1). The slope at time t is given by

$$\frac{\delta^{29}\text{Si}_{28,t+\delta t} - \delta^{29}\text{Si}_{28,t}}{\delta^{30}\text{Si}_{28,t+\delta t} - \delta^{30}\text{Si}_{28,t}}, \quad (3)$$

where δt is the size of the time step of the OMEGA+ simulation. The dashed line represents the slope of the presolar SiC grain

mainstream correlation line of 1.342 (T. Stephan et al. 2024). The dotted lines show the 95% confidence intervals of our simulations. Using the $^{28,29,30}\text{Si}$ (n, γ) reaction rates by K. H. Guber et al. (2003; top part of Figure 4), we find that the slope of the measured presolar SiC correlation line can be explained within the 95% confidence interval for all simulations younger than 3.5 Gyr prior to solar system formation. Moreover, the largest slope variation occurs at 2.7 Gyr prior to solar system formation. The majority of presolar SiC grains traveled through the ISM for short periods of time, e.g., up to 100 Myr (P. R. Heck et al. 2020). Only large and very rare presolar SiC grains were measured in the study of P. R. Heck et al. (2020). In contrast, our model–data comparison is mostly with measurements of smaller, micrometer-sized grains, for which no measured ages exist. Calculated survival times in the ISM are short (A. P. Jones & J. A. Nuth 2011), thus making an assumed 100 Myr lifetime for presolar grains a valid and conservative estimate. In addition, the silicon isotopes represent the original composition that the grains’ parent star started out with. Most mainstream grains likely originated from AGB stars with initial masses of 2–3 M_{\odot} (e.g., M. Lugaro et al. 2003). Assuming a simple mass–luminosity relation, we would thus expect the parent stars of these grains to have lived for about 0.6–1.8 Gyr. This roughly corresponds to GCE time steps between –1.9 and –0.9 Gyr in Figure 4. As shown in Figure 4, the spread in the predicted slope is large enough in this time span of interest to include the observed slope within the 95% confidence interval. Therefore, our model shows that nuclear reaction rate uncertainties can indeed explain the discrepancies between measurements and models. This conclusion is even stronger when using the reaction rates by Z. Y. Bao et al. (2000; bottom part of Figure 4). Here, all simulations agree within the 95% confidence interval with the measured presolar

grain slope. For the time range between -1.4 and -3.1 Ga, even the median slope agrees excellently between models and data.

Our results show that nuclear uncertainties significantly impact the GCE of silicon isotopes. In particular, we can reproduce the slope of the mainstream line within nuclear uncertainties. Our results, however, especially show the importance of the chosen $^{28,29,30}\text{Si}(n, \gamma)$ reaction rates. The $^{30}\text{Si}(n, \gamma)^{31}\text{Si}$ rate given by K. H. Guber et al. (2003) is 85% lower than the rate provided by Z. Y. Bao et al. (2000) at $kT = 8$ keV, which is similar to the temperature that stars reach in our simulations. Similarly, the $^{30}\text{Si}(n, \gamma)^{31}\text{Si}$ rate by H. Beer et al. (2002) would be about a factor of 2 higher than K. H. Guber et al. (2003), somewhere in between the rate used in the stellar simulations considered here. Those variations are well above the experimental uncertainties that we used in the individual cases, i.e., 2σ errors given by their reference sources, and our comparison between the rates of Z. Y. Bao et al. (2000) and K. H. Guber et al. (2003) clearly shows that the overall uncertainty in this rate is crucial to understand. In our scenario, the rate by Z. Y. Bao et al. (2000) seems to be preferred with respect to the one by K. H. Guber et al. (2003), since it leads to an excellent agreement with the presolar SiC grain data. E. Zinner et al. (2006) already concluded that using the Z. Y. Bao et al. (2000) nuclear cross sections results in a steeper slope in the silicon isotope GCE line than when using the rates by K. H. Guber et al. (2003). However, E. Zinner et al. (2006) also concluded that the K. H. Guber et al. (2003) nuclear reaction rates agree better with the ^{30}Si excesses in SiC Z grains. These grains likely originated from AGB stars. The ratios of the neutron-capture rates between K. H. Guber et al. (2003) and Z. Y. Bao et al. (2000) are 0.81 and 0.15 for $^{29}\text{Si}(n, \gamma)$ and $^{30}\text{Si}(n, \gamma)$ at 8 keV, respectively. Simply from these ratios, it is clear that the rates by Z. Y. Bao et al. (2000) will predict a steeper slope for the GCE correlation line and less ^{30}Si excess compared to the rates by K. H. Guber et al. (2003). While E. Zinner et al. (2006) prefer the rates by K. H. Guber et al. (2003) for the excess in ^{30}Si , they also state that other factors such as the temperature at the bottom of the He intershell and the mass-loss rate will significantly affect their conclusions. A future reevaluation of the comparison by E. Zinner et al. (2006) with newer AGB star models (e.g., M. Busso et al. 2021) would be desirable.

Our study suggests that a detailed evaluation of nucleosynthesis in O–C shell mergers is needed since it significantly affects the GCE of silicon isotopes. C. Ritter et al. (2018a) proposed that the observed Galactic trends of the odd-Z elements can be reproduced by increasing the O–C shell merger contributions in GCE. Our study shows that silicon isotopes in mainstream grains are also very sensitive to the nucleosynthesis in the O–C shell merger. Based on stellar models using the K. H. Guber et al. (2003) silicon neutron-capture cross sections by C. Ritter et al. (2018b), the occurrence of O–C shell mergers overproduces ^{30}Si , which is in stark contrast to presolar SiC mainstream grain measurements. On the other hand, and in contrast to all other GCE models we looked at, the O–C shell merger models predict the correct solar $^{29}\text{Si}/^{28}\text{Si}$. The contradicting evidence highlights the importance of a further investigation of both the relevant nuclear reaction rates discussed here and the dynamics and nucleosynthesis of the O–C shell mergers and their effects on GCE. Isotopic studies

represent a finer signature to study these effects than elemental abundances.

4. Conclusions

We presented an impact study of the effects of nuclear reaction rate uncertainties on the GCE of silicon isotopes and compared our results with measurements of presolar SiC mainstream grains. While currently no GCE model can adequately describe the measured isotope ratios and their distribution, we found for the first time that the slope of the simulated silicon isotope correlation agrees well with measurements of presolar SiC mainstream grains within nuclear reaction rate uncertainties. The slope of the silicon GCE trend agrees with the measurements within the 95% confidence interval when choosing the $^{28,29,30}\text{Si}(n, \gamma)$ rates by K. H. Guber et al. (2003). Using the higher rates by Z. Y. Bao et al. (2000) shows even better agreement; in fact, the expected average slope using these reaction rates agrees perfectly with the data.

Based on the stellar models available for this study, our results show that massive stars undergoing an O–C shell merger allow us to reproduce the solar ^{29}Si ratio with GCE simulations but overproduce ^{30}Si compared to the observations. C. Ritter et al. (2018a) found that a significant contribution from O–C mergers would be a possible solution to solve the underproduction of odd-Z elements in the Galaxy. In this work, we show that in the case of Si isotopes, the impact of O–C shell mergers is also relevant, but it is controversial.

Using Z. Y. Bao et al. (2000) or H. Beer et al. (2002) rates for the Si neutron-capture cross sections, CCSN models (and GCE models) would clearly predict lower amounts of ^{30}Si , which could potentially mitigate the discrepancy between GCE simulations and observations. Our findings thus underline the importance of future precision reaction rate measurements in order to finally solve this conundrum. New experimental data for these rates are paramount to define the role of O–C shell mergers in GCE. Isotope measurements are a very sensitive probe to study various stellar processes and should be considered in future GCE studies of the solar neighborhood.

Acknowledgments

We would like to thank James Cho for helpful discussion. M.P. is thankful for the support from the NKFI via K-project 138031 and the Lendület Program LP2023-10 of the Hungarian Academy of Sciences. We acknowledge the support to NuGrid from JINA-CEE (NSF Grant PHY-1430152) and ongoing access to *viper*, the University of Hull High Performance Computing Facility. M.P. and R.T. acknowledge the support from the European Union’s Horizon 2020 research and innovation program (ChETEC-INFRA—project No. 101008324) and the IRENA network supported by US NSF AccelNet (grant No. OISE-1927130).

Software: `matplotlib` (J. D. Hunter 2007), `NumPy` (C. R. Harris et al. 2020), `SciPy` (P. Virtanen et al. 2020), `pandas` (W. McKinney 2010; The pandas development team 2020).

Appendix A

Mass Coordinates of Relevant Silicon Production Zones

Table 2 shows the mass coordinates of the O-burning zone in all massive star models by C. Ritter et al. (2018b).

Table 2

Mass Coordinates of Stellar Zones Where Explosive Oxygen Burning Takes Place in Stellar Models by C. Ritter et al. (2018b) of Given Mass and Metallicity

Mass (M_{\odot})	Metallicity	Mass Coordinate Range (M_{\odot})
12	0.01	2.12–2.78
12	0.02	1.96–2.43
25	0.01	6.05–9.19
25	0.02	6.55–8.96

Appendix B Trajectories

For all stellar models, we take representative 1D temperature, plasma-density trajectories from the respective silicon production zones, ranging from mass coordinates m_a to m_b . The subscript represents the index of the computational grid of the MESA stellar evolution code, where 0 represents the center of the star. For all stellar models, 21 trajectories equally spaced in index space are taken. For the stellar model with $M/M_{\odot} = 25$, $Z = 0.01$, five additional trajectories equally spaced in index space are taken between mass coordinates 6.852 and 7.219 M_{\odot} to capture all the silicon isotope production peaks. The dashed lines in Figure 5 show the representative trajectories taken. The solid lines represent the difference between the postsupernova and presupernova silicon isotopic abundances.

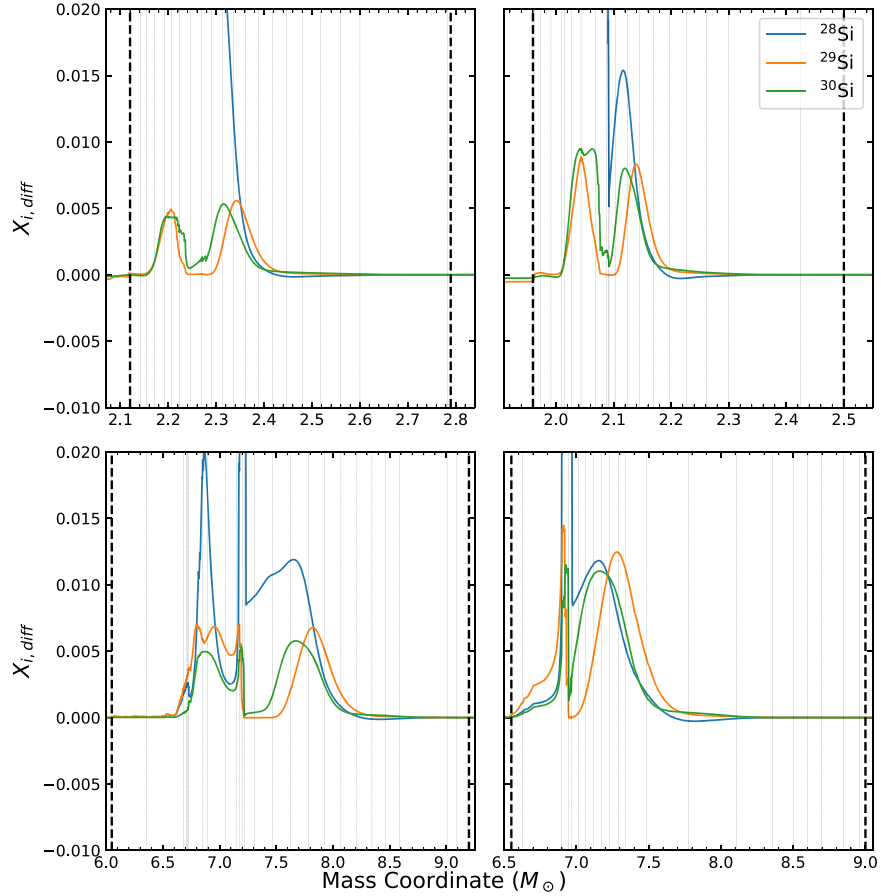


Figure 5. Isotopic abundances of silicon isotopes at a given mass coordinate for representative 1D trajectories taken for the 12 M_{\odot} (top) and 25 M_{\odot} (bottom) stars for $Z = 0.01$ (left) and $Z = 0.02$ (right).

Appendix C Convergence of MC Simulations

The convergence of the MC simulations is tested using the distribution of the silicon isotope correlation lines at $t = -2.3$ Gyr with increasing sample size N_{MC} . Figure 6 shows the means of the distribution with sample size N_{MC} , where $N_{MC} \in \{100, 110, 120, \dots, 10,000\}$. We see that the estimated mean stabilizes as N_{MC} increases. We estimate the point of convergence through a bootstrapping technique, a statistical procedure that generates a set of simulated samples by sampling from an existing sample with replacement. It is generally used to estimate the accuracy of sample estimates such as mean and median. The exact procedure we use is

as follows. First, we take a sample of size $N_{MC} \in \{100, 200, 300, \dots, 10,000\}$ from the 10,000 MC results. Then, we generate 10,000 simulated samples of size N_{MC} by sampling from the sample of MC results with replacement and calculate the mean of each simulated sample. Finally, we calculate the standard deviation of the means of the 10,000 simulated samples. Figure 6 shows the calculated standard deviations for all N_{MC} . The estimated standard deviations of the sample means monotonically decrease as N_{MC} increases, suggesting that the MC simulations we performed are converging. When $N_{MC} = 10,000$, the standard deviation of the sample mean estimated by the bootstrapping method is ~ 0.003 , which is $< 0.5\%$ of the sample mean, suggesting that the convergence of the MC simulation at $N_{MC} = 10,000$.

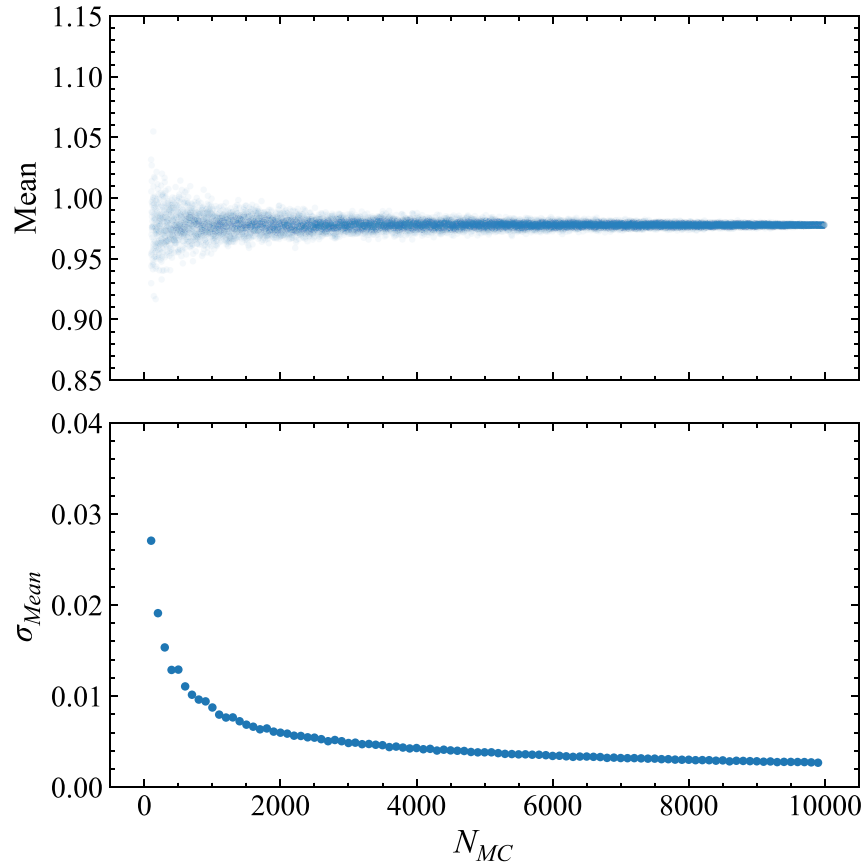


Figure 6. Convergence test of our MC model. Clearly, the mean silicon isotope correlation lines have converged well at our chosen value after several thousand MC runs, showing that our results will not change when running more than 10,000 simulations.

Appendix D Silicon Production Variations within the Relevant Zones

Figure 7 shows the variations of the postsupernova silicon isotopic abundances in the silicon production zones for selected massive star models. The solid lines represent the postsupernova compositions in the default stellar nucleosynthesis models (C. Ritter et al. 2018b), i.e., without reaction rate variations.

The shaded areas show the whole range of variance as determined by our MC simulations, with dotted contours marking the 95% confidence intervals. The largest variation shows up in the results for ^{29}Si due to large uncertainties in the nuclear reaction rates. Final isotopic abundances in the oxygen-burning zones can vary more than an order of magnitude. On the other hand, ^{28}Si and ^{30}Si show less variation due to reaction rate uncertainties.

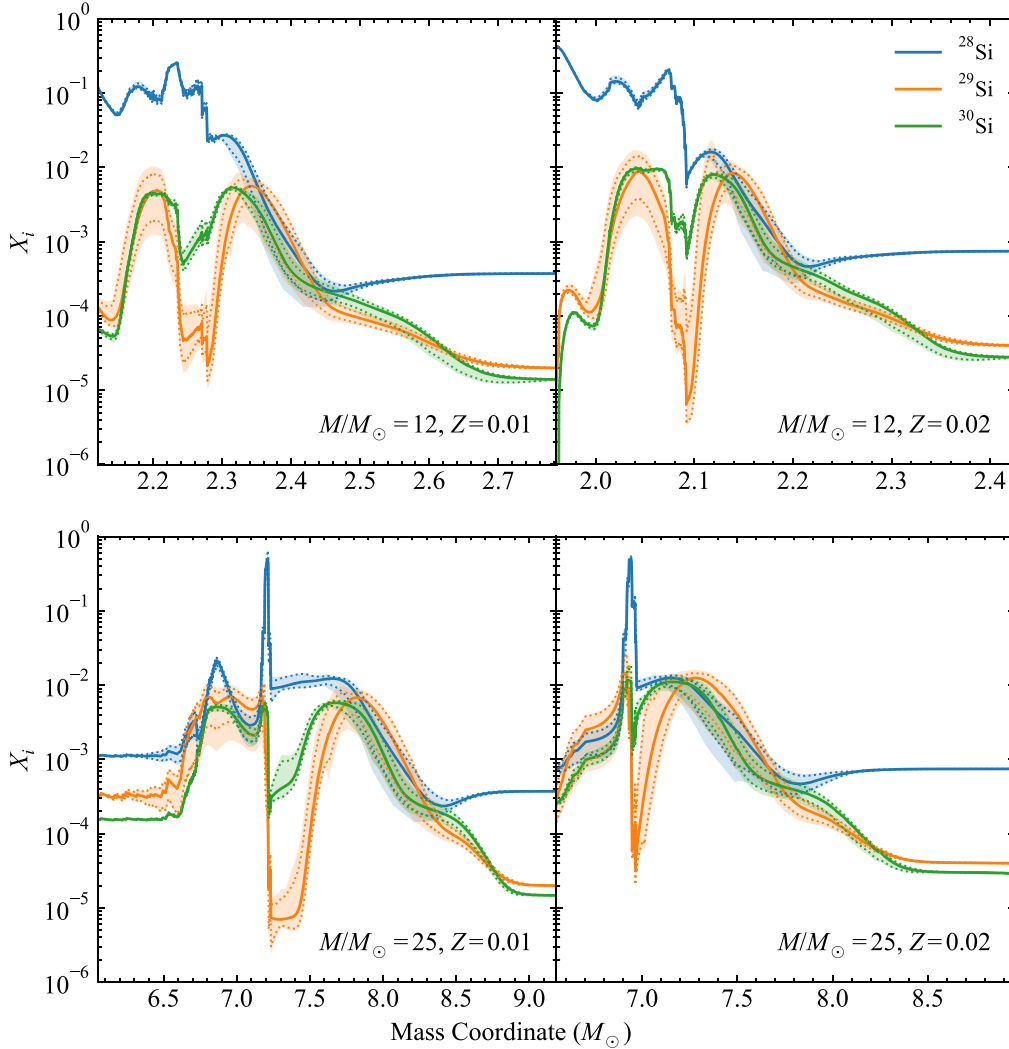






Figure 7. Silicon abundance at the end of the CCSN explosion within the explosive silicon production zone of the $12 M_\odot$ (top) and $25 M_\odot$ (bottom) stars for $Z = 0.01$ (left) and $Z = 0.02$ (right). Lines represent the unmodified abundance, as in C. Ritter et al. (2018b). Shaded areas show the overall range for 10,000 MC simulations while varying the nuclear reactions rates, while the dotted lines show the 95% confidence interval of our MC simulations.

ORCID iDs

Hung Kwan Fok  <https://orcid.org/0009-0008-6833-7300>
 Marco Pignatari  <https://orcid.org/0000-0002-9048-6010>
 Benoît Côté  <https://orcid.org/0000-0002-9986-8816>
 Reto Trappitsch  <https://orcid.org/0000-0002-0924-236X>

References

- Alexander, C. M. O'D., & Nittler, L. R. 1999, *ApJ*, 519, 222
 Amari, S., Lewis, R. S., & Anders, E. 1994, *GeCoA*, 58, 459
 Andrassy, R., Herwig, F., Woodward, P., & Ritter, C. 2020, *MNRAS*, 491, 972
 Bao, Z. Y., Beer, H., Käppeler, F., et al. 2000, *ADNDT*, 76, 70
 Beer, H., Sedyshev, P. V., Rochow, W., Rauscher, T., & Mohr, P. 2002, *NuPhA*, 709, 453
 Busso, M., Vescovi, D., Palmerini, S., Cristallo, S., & Antonuccio-Delogu, V. 2021, *ApJ*, 908, 55
 Clayton, D. D. 2003, *ApJ*, 598, 313
 Clayton, D. D., & Timmes, F. X. 1997, *ApJ*, 483, 220
 Côté, B., Lugaro, M., Reifarth, R., et al. 2019, *ApJ*, 878, 156
 Côté, B., O'Shea, B. W., Ritter, C., Herwig, F., & Venn, K. A. 2017, *ApJ*, 835, 128
 Côté, B., Silvia, D. W., O'Shea, B. W., Smith, B., & Wise, J. H. 2018, *ApJ*, 859, 67
 Fryer, C. L., Belczynski, K., Wiktorowicz, G., et al. 2012, *ApJ*, 749, 91
 Gallino, R., Arlandini, C., Busso, M., et al. 1998, *ApJ*, 497, 388
 Grevesse, N., & Noels, A. 1993, in *Origin and Evolution of the Elements*, ed. N. Prantzos, E. Vangioni-Flam, & M. Casse (Heidelberg: Astronomisches Rechen-Institut), 15
 Guber, K. H., Koehler, P. E., Derrien, H., et al. 2003, *PhRvC*, 67, 062802
 Harris, C. R., Millman, K. J., van der Walt, S. J., et al. 2020, *Natur*, 585, 357
 Heck, P. R., Greer, J., Kööp, L., et al. 2020, *PNAS*, 117, 1884
 Hoppe, P., Annen, P., Strebler, R., et al. 1997, *ApJL*, 487, L101
 Hoppe, P., Leitner, J., Meyer, B. S., et al. 2009, *ApJL*, 691, L20
 Hunter, J. D. 2007, *CSE*, 9, 90
 Jones, A. P., & Nuth, J. A. 2011, *A&A*, 530, A44
 Kobayashi, C., Karakas, A. I., & Lugaro, M. 2020, *ApJ*, 900, 179
 Limongi, M., & Chieffi, A. 2018, *ApJS*, 237, 13
 Liu, N., Savina, M. R., Davis, A. M., et al. 2014, *ApJ*, 786, 66
 Loders, K. 2021, *SSRv*, 217, 44
 Lugaro, M., Davis, A. M., Gallino, R., et al. 2003, *ApJ*, 593, 486
 Lugaro, M., Zinner, E., Gallino, R., & Amari, S. 1999, *ApJ*, 527, 369
 Magg, E., Bergemann, M., Serenelli, A., et al. 2022, *A&A*, 661, A140
 McKinney, W. 2010, in *Proc. 9th Python in Science Conf.*, ed. S. van der Walt & J. Millman, 56
 Merrill, P. W. 1952, *ApJ*, 116, 21
 Nittler, L. R. 2005, *ApJ*, 618, 281
 Nittler, L. R., & Ciesla, F. 2016, *ARA&A*, 54, 53
 Nomoto, K., Kobayashi, C., & Tominaga, N. 2013, *ARA&A*, 51, 457
 Paxton, B., Bildsten, L., Dotter, A., et al. 2011, *ApJS*, 192, 3
 Paxton, B., Cantiello, M., Arras, P., et al. 2013, *ApJS*, 208, 4
 Paxton, B., Marchant, P., Schwab, J., et al. 2015, *ApJS*, 220, 15
 Pignatari, M., Herwig, F., Hirschi, R., et al. 2016, *ApJS*, 225, 24
 Rauscher, T., Nishimura, N., Hirschi, R., et al. 2016, *MNRAS*, 463, 4153
 Ritter, C., Andrassy, R., Côté, B., et al. 2018a, *MNRAS: Letters*, 474, L1
 Ritter, C., Herwig, F., Jones, S., et al. 2018b, *MNRAS*, 480, 538
 Roberti, L., Limongi, M., & Chieffi, A. 2024, *ApJS*, 270, 28
 Savina, M. R., Davis, A. M., Tripa, C. E., et al. 2004, *Sci*, 303, 649
 Stephan, T., Trappitsch, R., Hoppe, P., et al. 2024, *ApJS*, 270, 27
 The pandas development team 2020, pandas-dev/pandas: Pandas, v2.2.2, Zenodo, doi: 10.5281/zenodo.3509134
 Timmes, F. X., & Clayton, D. D. 1996, *ApJ*, 472, 723
 Virtanen, P., Gommers, R., Oliphant, T. E., et al. 2020, *NatMe*, 17, 261
 Womack, K. A., Vincenzo, F., Gibson, B. K., et al. 2022, *MNRAS*, 518, 1543
 Zinner, E., Nittler, L. R., Gallino, R., et al. 2006, *ApJ*, 650, 350